FDTD Simulation von Elektronenstreuung an einer elektromagnetischen Welle

FDTD Simulation of electron scattering in an electromagnetic wave

David Symhoven

München 2017

FDTD Simulation von Elektronenstreuung an einer elektromagnetischen Welle

FDTD Simulation of electron scattering in an electromagnetic wave

David Symhoven

Masterarbeit
am Lehrstuhl Computational & Plasma Physics
der Ludwig–Maximilians–Universität
München

vorgelegt von
David Symhoven
aus Witten

München, den 18.07.2017

Erstgutachter: Prof.Dr.Hartmut Ruhl
Zweitgutachter: Zweitgutachter

Introduction

Now it's going loose ...[1]
What is the goal of this thesis?
What is Plasma, and where is it used ?
Summary of all chapters

Symbols and Constants

Vacuum permittivity	ϵ_0	$8.85418781762 \cdot 10^{-12}\ \mathrm{A\,s\,V^{-1}\,m^{-1}}$
Vacuum permeability	μ_0	$2566370614 \cdot 10^{-6}\ \mathrm{N\,A^{-2}}$
Speed of Light	c	$299792458\ \mathrm{m\,s^{-1}}$
Electrical flux density	$\vec{D}$	$[\mathrm{A\,s\,m^{-2}}]$
Magnetic flux density	$\vec{B}$	[T]
Magnetic field strength	$\vec{H}$	$[\mathrm{A\,m^{-1}}]$
Electric field stength	$\vec{E}$	$[\mathrm{V\,m^{-1}}]$
Poynting Vector	$\vec{S}$	$[\mathrm{N\,m^{-1}\,s^{-1}}]$
Position	$\vec{r}$	[m]
Velocity	$\vec{v}$	$[\mathrm{m\,s^{-1}}]$
Normalized Velocity	$\vec{\beta} = \frac{\vec{v}}{c}$	[]
Normalized Acceleration	$\dot{\vec{\beta}}$	$[\mathrm{s^{-1}}]$
Wavelength	λ	[m]
Wavevector	$\vec{k}$	$[\mathrm{m^{-1}}]$
Time	t	[s]
discretized Time	h	[s]
Frequenzy	ω	$[\mathrm{s^{-1}}]$
Nabla - Operator	$\vec{\nabla}$	$\left(\frac{\partial}{\partial r_1}, \ldots, \frac{\partial}{\partial r_n}\right)$
Laplace - Operator	Δ	$\sum_{i=1}^{n} \frac{\partial^2}{\partial r_i^2}$
d'Alembert - Operator	$\hat{\Box}$	$\Delta - \frac{1}{c^2}\frac{\partial^2}{\partial t^2}$

Contents

Part I.

Fundamentals

In this first part we present the theoretical basics this thesis is built upon. We start with the foundation of electromagnetism - the Maxwell Equations - followed by the corresponding potential equations. Introducing Lorentz-Gauge will lead us to the inhomogeneous wave equation, which we will solve using Greens-function approach. This will lead us to the Liénard-Wiechert potentials, which are key in this thesis. Lastly we discuss both the non relativistic and relativistic phenomenon of energy radiation, where we restrict ourselves to the simple case where a particle is accelerated parallel to its direction of motion.

1

Electromagnetic radiation

1.1 Maxwell-Equations

The Maxwell equations are the foundation of the classical electromagnetism and describe how the electric field strength $\vec{E} \in \mathbb{R}^3$ and the magnetic field strength $\vec{H} \in \mathbb{R}^3$ are generated by charges and currents respectively and how they evolve over time in space in presence of one another. In presence of matter however, the interaction of the fields with the material need to be taken into account. The effect of microscopic dipols, formed by bound charge carriers, are summarized in macroscopic entities called Polarisation $\vec{P} \in \mathbb{R}^3$ and Magnetization $\vec{M} \in \mathbb{R}^3$. These dipols align in the external field such that the resulting electric and magnetic field are described by

$$\begin{aligned} \vec{D} &:= \epsilon_0 \vec{E} + \vec{P} \\ \vec{H} &:= \frac{1}{\mu_0} \vec{B} - \vec{M}, \end{aligned} \tag{1.1}$$

where μ_0 and ϵ_0 are the vacuum permeability and permittivity respectively. The macroscopic Maxwell Equations than read

$$\vec{\nabla} \vec{B} = 0 \tag{1.2}$$

$$\vec{\nabla} \vec{D} = \rho \tag{1.3}$$

$$\vec{\nabla} \times \vec{E} = -\frac{\partial \vec{B}}{\partial t} \tag{1.4}$$

$$\vec{\nabla} \times \vec{H} = \frac{\partial \vec{D}}{\partial t} + \vec{j}, \tag{1.5}$$

where ρ denotes the charge density of the electric source and $\vec{j}$ the electric current density. In the case of vacuum, the material equations (1.1) reduce to

$$\begin{aligned} \vec{D} &= \epsilon_0 \vec{E} \\ \vec{H} &= \frac{1}{\mu_0} \vec{B}. \end{aligned} \tag{1.6}$$

1.2 Colomb and Lorentz Gauge

In the following section we consider the Maxwell Equations in vacuum.
The electric and magnetic fields can also be described by a scalar and a vector potential respectively. From (1.2) we can conclude that

$$\exists \vec{A} \in \mathbb{R}^3 \colon \vec{B} = \vec{\nabla} \times \vec{A}, \tag{1.7}$$

where $\vec{A}$ is called the vector potential. Plugging in (1.7) into (1.4) yields

$$\begin{aligned} \vec{\nabla} \times \left(\vec{E} + \frac{\partial \vec{A}}{\partial t} \right) &= 0. \\ \Rightarrow \exists \varphi \in \mathbb{R} \colon \vec{E} + \frac{\partial \vec{A}}{\partial t} &= -\vec{\nabla}\varphi. \end{aligned} \tag{1.8}$$

φ is called scalar potential. Plugging in (1.8) into (1.3) and also (1.7) and (1.8) into (1.5) gives the potential equations

$$\begin{aligned} -\Delta\varphi - \vec{\nabla}\left(\frac{\partial \vec{A}}{\partial t} \right) &= \frac{\rho}{\epsilon_0} \\ \underbrace{\left(\Delta - \frac{1}{c^2}\frac{\partial^2}{\partial t^2} \right)}_{:=\hat{\Box}} \vec{A} - \vec{\nabla}\left(\vec{\nabla}\vec{A} + \frac{1}{c^2}\frac{\partial \varphi}{\partial t} \right) &= -\mu_0 \vec{j}, \end{aligned} \tag{1.9}$$

where we used the *Graßmann Identity*: $\vec{\nabla} \times (\vec{\nabla} \times \vec{A}) = \vec{\nabla}(\vec{\nabla}\vec{A}) - \Delta\vec{A}$.
The description of the fields by the aforementioned potentials φ and $\vec{A}$ are not unique. This is called gauge freedom. The potentials can be specifically adjusted to the problem at hand. The gauge transformations look like

$$\begin{aligned} \vec{A} &\mapsto \vec{A}' = \vec{A} + \vec{\nabla}\psi \\ \varphi &\mapsto \varphi' = \varphi - \frac{\partial \psi}{\partial t}, \end{aligned} \tag{1.10}$$

where $\psi \colon \mathbb{R}^3 \times \mathbb{R} \mapsto \mathbb{R}$. In appendix A we show, that ψ does indeed not change the physics.

If we choose ψ such that

$$\vec{\nabla}\vec{A} + \frac{1}{c^2}\frac{\partial \varphi}{\partial t} = 0, \tag{1.11}$$

then we call it a *Lorentz Gauge* and the potential Equations (1.9) decouple into two separate wave equations

$$\begin{aligned} \hat{\Box}\varphi &= -\frac{\rho}{\epsilon_0} \\ \hat{\Box}\vec{A} &= -\mu_0 \vec{j}. \end{aligned} \tag{1.12}$$

1.3 Liénard-Wiechert Potentials

1.3.1 Solution of inhomogeneous wave equation

The *Liénard-Wiechert* Potentials are the solution of (1.12). Following[6] we solve the general case

$$\hat{\Box}\psi(\vec{r},t) = f(\vec{r},t), \tag{1.13}$$

where $\psi, f : \mathbb{R}^3 \times \mathbb{R} \mapsto \mathbb{R}$. f is called source function and will be specified later. (1.13) is a linear inhomgeneous partial differential equation. Those kind of equations are solved with the *Green's function* approach. If we can find the Green's function G fulfilling

$$\hat{\Box}G(\vec{r}-\vec{r}\,',t-t') = -\delta(\vec{r}-\vec{r}\,')\delta(t-t'), \tag{1.14}$$

then we can calculate the solution of (1.13) via

$$\psi(\vec{r},t) = \int\int G(\vec{r}-\vec{r}',t-t')f(\vec{r},t)\mathrm{d}t'\ \mathrm{d}\vec{r}\,'. \tag{1.15}$$

To find G we use the following Fourier - Transformations

$$\begin{aligned} G(\vec{r}-\vec{r}\,',t-t') &= \frac{1}{4\pi^2}\int\int G(\vec{k},\omega)\exp(i\vec{k}(\vec{r}-\vec{r}\,'))\exp(-i\omega(t-t'))\mathrm{d}\omega\ \mathrm{d}\vec{k}, \\ \delta(\vec{r}-\vec{r}\,') &= \frac{1}{4\pi^2}\int \exp(i\vec{k}(\vec{r}-\vec{r}\,'))\mathrm{d}\vec{k}, \\ \delta(t-t') &= \frac{1}{4\pi^2}\int \exp(-i\omega(t-t'))\mathrm{d}\omega. \end{aligned} \tag{1.16}$$

Plugging in (1.16) into (1.14) yields

$$\int\int \exp(i\vec{k}(\vec{r}-\vec{r}\,'))\exp(-i\omega(t-t'))\left[G(\vec{k},\omega)\left(-k^2+\frac{\omega^2}{c^2}\right)+\frac{1}{4\pi^2}\right] = 0,$$

which leaves us with

$$G(\vec{k},\omega) = \frac{1}{4\pi^2}\frac{1}{k^2 - \frac{\omega^2}{c^2}}.$$

Using residue theorem we find the Fourier Back Transform of G to be

$$G_{ret}(\vec{r}-\vec{r}\,',t-t') = \frac{\delta(t'-t_{ret})}{4\pi|\vec{r}-\vec{r}\,'|}, \tag{1.17}$$

where

$$t_{ret} \coloneqq t - \frac{|\vec{r}-\vec{r}\,'|}{c} \tag{1.18}$$

is the retarded time. We also call G_{ret} the *retarded Green's function* in contrast to the *advanced Green's function* G_{av} with the advanced time

$$t_{av} \coloneqq t + \frac{|\vec{r}-\vec{r}\,'|}{c}. \tag{1.19}$$

The latter does not fulfill the causal principle of physics. We expect the reason for a change in our signal at $\vec{r}$ at time t, due to a perturbation, to be in the past, not the future. Because $t_{ret} < t$ the retarded Green's function is the one to work with. Plugging in (1.17) into (1.15) yields

$$\psi(\vec{r},t) = \frac{1}{4\pi}\int \frac{f(\vec{r}\,',t_{ret})}{|\vec{r}-\vec{r}\,'|}\mathrm{d}\vec{r}\,', \tag{1.20}$$

which finally leads to the retarded potential equations

$$\varphi(\vec{r},t) = \frac{1}{4\pi\epsilon_0}\int \frac{\rho(\vec{r}\,',t_{ret})}{|\vec{r}-\vec{r}\,'|}\mathrm{d}\vec{r}\,', \tag{1.21}$$

$$\vec{A}(\vec{r},t) = \frac{\mu_0}{4\pi}\int \frac{\vec{j}(\vec{r}\,',t_{ret})}{|\vec{r}-\vec{r}\,'|}\mathrm{d}\vec{r}\,'. \tag{1.22}$$

Lastly we show in Appendix B that they indeed fulfill the Laurentz Gauge (1.11).

1.3.2 Special Case: Moving point charge

Now we want to discuss the special case of a particle with charge q, moving along the trajectory $\vec{r}_p$ with velocity $\vec{v} \coloneqq \dot{\vec{r}}_p$, where the dot donates the time derivative. As

mentioned before, we now define the source functions for our problem at hand. For the charge density we have

$$\rho(\vec{r},t) = q\delta(\vec{r} - \vec{r}_p(t)) \tag{1.23}$$

and for the current density

$$\vec{j}(\vec{r},t) = q\vec{v}\delta(\vec{r} - \vec{r}_p(t)). \tag{1.24}$$

Identifying

$$\begin{aligned}\psi(\vec{r},t) &= \varphi(\vec{r},t) \text{ and } f(\vec{r}\,',t') = \frac{\rho(\vec{r}\,',t')}{\epsilon_0},\\ \vec{\psi}(\vec{r},t) &= \vec{A}(\vec{r},t) \text{ and } \vec{f}(\vec{r}\,',t') = \mu_0\vec{j}(\vec{r}\,',t')\end{aligned}$$

and using (1.15) with (1.17) yields after integrating over $\vec{r}\,'$

$$\begin{aligned}\varphi(\vec{r},t) &= \frac{1}{4\pi\epsilon_0}\int \frac{\delta\left(\frac{|\vec{r}-\vec{r}_p|}{c} - t + t'\right)}{|\vec{r}-\vec{r}_p|}\mathrm{d}t',\\ \vec{A}(\vec{r},t) &= \frac{q\mu_0}{4\pi}\int \vec{v}(t')\frac{\delta\left(\frac{|\vec{r}-\vec{r}_p|}{c} - t + t'\right)}{|\vec{r}-\vec{r}_p|}\mathrm{d}t'.\end{aligned} \tag{1.25}$$

For the t' - integration we need the following property of the δ - distribution

$$\delta\left[g(t')\right] = \sum_{i=1}^{n}\frac{\delta(t'-t_i)}{\left|\left(\frac{\mathrm{d}g}{\mathrm{d}t'}\right)\Big|_{t'=t_i}\right|}, \tag{1.26}$$

where

$$g(t') \coloneqq \frac{|\vec{r}-\vec{r}_p|}{c} - t + t' \tag{1.27}$$

and t_i are the roots of g. To find the roots of g, let's consider

$$\begin{aligned}\frac{\mathrm{d}g}{\mathrm{d}t'} &= 1 + \frac{1}{c}\frac{\mathrm{d}}{\mathrm{d}t'}|\vec{r}-\vec{r}_p| = 1 - \frac{\vec{v}(t')}{c}\underbrace{\frac{\vec{r}-\vec{r}_p}{|\vec{r}-\vec{r}_p|}}_{|\cdot|=1}\\ &\Longrightarrow 1 - \frac{\vec{v}(t')}{c} \le \frac{\mathrm{d}g}{\mathrm{d}t'} \le 1 + \frac{\vec{v}(t')}{c}\\ &\overset{v<c}{\Longrightarrow} \frac{\mathrm{d}g}{\mathrm{d}t'} > 0,\end{aligned} \tag{1.28}$$

which means that g is a monotonically increasing function and therefore has at most one root, which is $t' = t_{ret}$ as can be seen from (1.27). In case that g has no roots at all, we can conclude that $\varphi \equiv 0$ and $\vec{A} \equiv 0$.
With $t_{ret} \coloneqq t - \frac{|\vec{r}-\vec{r}_p|}{c}$ the integration over t' yields

$$\begin{aligned}\varphi(\vec{r},t) &= \frac{1}{4\pi\epsilon_0}\frac{q}{|\vec{r}-\vec{r}_p(t_{ret})| - \frac{\vec{v}(t_{ret})}{c}(\vec{r}-\vec{r}_p(t_{ret}))},\\ \vec{A}(\vec{r},t) &= \frac{1\mu_0}{4\pi}\frac{q\vec{v}(t_{ret})}{|\vec{r}-\vec{r}_p(t_{ret})| - \frac{\vec{v}(t_{ret})}{c}(\vec{r}-\vec{r}_p(t_{ret}))}\end{aligned} \tag{1.29}$$

which are the *Liénard-Wiechert* Potentials. Upon defining

$$\begin{aligned}\vec{\beta}(t) &\coloneqq \frac{\vec{v}(t)}{c},\\ \vec{R}(\vec{r},t) &\coloneqq \vec{r}-\vec{r}_p(t),\\ \vec{n}(\vec{r},t) &\coloneqq \frac{\vec{R}(\vec{r},t)}{R(\vec{r},t)}\end{aligned} \tag{1.30}$$

we can rewrite the Liénard-Wiechert Potentials in a more compact and final form

$$\begin{aligned}\varphi(\vec{r},t) &= \frac{1}{4\pi\epsilon_0}\frac{q}{(1-\vec{\beta}(t')\cdot\vec{n}(\vec{r},t'))R(\vec{r},t')}\bigg|_{t'=t_{ret}},\\ \vec{A}(\vec{r},t) &= \frac{\mu_0}{4\pi}\frac{q\vec{\beta}(t')}{(1-\vec{\beta}(t')\cdot\vec{n}(\vec{r},t'))R(\vec{r},t')}\bigg|_{t'=t_{ret}}.\end{aligned} \tag{1.31}$$

They are the generalization of the Coulomb Potential. With the help of (1.8) the electric and magnetic fields can be derived from the *Liénard-Wiechert* Potentials (1.31). Since this is a quite longish calculation we refer to[6] and just present the final result

$$\begin{aligned}\vec{E}(\vec{r},t) &= \frac{q}{4\pi\epsilon_0}\left(\frac{\vec{n}(\vec{r},t')-\vec{\beta}(t)}{\gamma^2(1-\vec{\beta}(t)\cdot\vec{n}(\vec{r},t'))^3R^2(\vec{r},t')}\right.\\ &\qquad\left.+\frac{1}{c}\frac{\vec{n}(\vec{r},t')\times(\vec{n}(\vec{r},t')-\vec{\beta}(t))\times\dot{\vec{\beta}}(t)}{(1-\vec{\beta}(t)\cdot\vec{n}(\vec{r},t'))^3R(\vec{r},t')}\right)\bigg|_{t'=t_{ret}},\\ \vec{B}(\vec{r},t) &= \frac{1}{c}\left(\vec{n}(\vec{r},t')\times\vec{E}(\vec{r},t)\right)\bigg|_{t'=t_{ret}}.\end{aligned} \tag{1.32}$$

This is the electric and magnetic field of a moving charged particle. Due to the finite speed of light, the fields need time to travel from their source to the observation point. That means, that the fields at time t, were actually produced at a earlier time t_{ret}. As can be seen in figure 3.1, the retarded time is determined by the intersection point of the particle trajectory with the backward lightcone of the observation point.

1.3.3 Energy emission

Now we want to discuss the energy flow and emission. Therefore we need to analyze the Poynting Vector

$$\vec{S} = \frac{1}{\mu_0}\vec{E} \times \vec{B} = \frac{1}{\mu_0 c}\left[\vec{n}_{ret}E^2 - \left(\vec{n}_{ret}\vec{E}\right)\vec{E}\right], \tag{1.33}$$

where $\vec{n}_{ret} \coloneqq \vec{n}(\vec{r}, t_{ret})$. Taking a closer look at (1.32) reveals that both $\vec{E}$ and $\vec{B}$ can be separated into two parts, one of which is not dependent on the particle acceleration

$$\begin{aligned}
\vec{E}_{(v)}(\vec{r},t) &= \frac{q}{4\pi\epsilon_0}\frac{1}{\gamma^2(1-\vec{\beta}(t')\cdot\vec{n}(\vec{r},t'))^3R^2(\vec{r},t')}\left(\vec{n}(\vec{r},t')-\vec{\beta}(t')\right)\Big|_{t'=t_{ret}} \\
\vec{B}_{(v)}(\vec{r},t) &= \frac{q}{4\pi\epsilon_0 c}\frac{1}{\gamma^2(1-\vec{\beta}(t')\cdot\vec{n}(\vec{r},t'))^3R^2(\vec{r},t')}\underbrace{\left[\vec{n}\times\left(\vec{n}(\vec{r},t')-\vec{\beta}(t')\right)\right]}_{=\frac{1}{c}(\vec{v}\times\vec{n})}\Big|_{t'=t_{ret}}
\end{aligned} \tag{1.34}$$

whilst the other is through $\dot{\vec{\beta}}$

$$\begin{aligned}
\vec{E}_{(a)}(\vec{r},t) &= \frac{q}{4\pi\epsilon_0 c}\frac{\vec{n}(\vec{r},t')\times\left(\vec{n}(\vec{r},t')-\vec{\beta}(t')\right)\times\dot{\vec{\beta}}(t')}{\left(1-\vec{\beta}(t')\cdot\vec{n}(\vec{r},t')\right)^3R(\vec{r},t')}\Big|_{t'=t_{ret}} \\
\vec{B}_{(a)}(\vec{r},t) &= \frac{q}{4\pi\epsilon_0 c^2}\frac{\vec{n}(\vec{r},t')\times\left[\vec{n}(\vec{r},t')\times\left(\vec{n}(\vec{r},t')-\vec{\beta}(t')\right)\times\dot{\vec{\beta}}(t')\right]}{\left(1-\vec{\beta}(t')\cdot\vec{n}(\vec{r},t')\right)^3R(\vec{r},t')}\Big|_{t'=t_{ret}}.
\end{aligned} \tag{1.35}$$

Since $E_{(v)} \propto \frac{1}{R^2}$ whereas $E_{(a)} \propto \frac{1}{R}$, its field contributions will dominate in the far field, i.e. for large distances from the source. Plugging in (1.32) in (1.33) gives us several terms

with different orders of $\frac{1}{R}$, namely

$$\vec{S}_{vv} \propto \left|\vec{E}_{(v)} \times \vec{B}_{(v)}\right| \propto \frac{1}{R^4},$$
$$\vec{S}_{va} \propto \left|\vec{E}_{(v)} \times \vec{B}_{(a)}\right| \propto \frac{1}{R^3},$$
$$\vec{S}_{aa} \propto \left|\vec{E}_{(a)} \times \vec{B}_{(a)}\right| \propto \frac{1}{R^2}.$$

By evaluating the energy flux through an arbitrary surface with differential surface area $\mathrm{d}\vec{\sigma}$, as illustrated in figure 1.1,

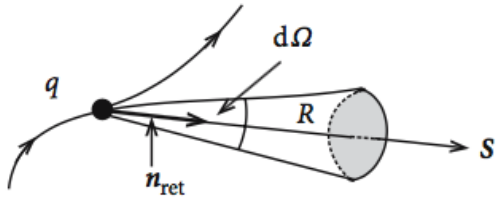

Figure 1.1.: Illustration of how to calculate the energy emission of a moving particle with charge q.[6]

we can see, that it will suffice to only consider the $\frac{1}{R^2}$ terms, because the $\frac{1}{R^3}$ or higher terms do not contribute to the energy emission, since

$$\oint \vec{S}\mathrm{d}\vec{\sigma} \rightsquigarrow \oint \frac{1}{R^3} r^2 \mathrm{d}\Omega \rightsquigarrow \oint \frac{1}{r}\mathrm{d}\Omega \rightsquigarrow \frac{1}{r} \overset{r\to\infty}{\longrightarrow} 0, \tag{1.36}$$

where $\mathrm{d}\Omega \coloneqq \sin(\vartheta)\mathrm{d}\vartheta\mathrm{d}\varphi$. That means we can focus on (1.35) when calculating (1.33)

$$\vec{S} = \frac{1}{\mu_0 c}\frac{q^2}{16\pi^2\epsilon_0^2 c^2}\frac{\vec{n}(\vec{r},t')\left[\vec{n}(\vec{r},t') \times \left(\vec{n}(\vec{r},t') - \vec{\beta}(t')\right) \times \dot{\vec{\beta}}(t')\right]^2}{\left(1 - \vec{\beta}(t')\cdot\vec{n}(\vec{r},t')\right)^6 R^2(\vec{r},t')}\Bigg|_{t'=t_{ret}} + \mathcal{O}\left(\frac{1}{R^3}\right) \tag{1.37}$$

The energy flux has the direction of $\vec{n}_{ret}$, i.e. it flows from the particle position $\vec{r}_p$ at time $t' = t_{ret}$ to the observation point $\vec{r}$. We can also see, that only accelerated particles ($\dot{\vec{\beta}} \neq 0$) loose energy through radiation, which leads to a reduction in kinetic energy. Although an uniformly moving particle produces E and B - fields, it does not loose energy

through radiation.

Lastly we want to discuss the radiation power. The emitted energy per time $\mathrm{d}t$ into the solid angle $\mathrm{d}\Omega$ is described by

$$\frac{\mathrm{d}W}{\mathrm{d}\Omega} = \left(\vec{S}\cdot\vec{n}(\vec{r},t')\right) R^2(\vec{r},t')\Big|_{t'=t_{ret}}. \tag{1.38}$$

Usually the observed amount of energy per unit time $\mathrm{d}t$ is not the same as the emitted energy of the particle per unit time $\mathrm{d}t_{ret}$. To learn more about the emission within the particles system, we want to express our equation in terms of $\mathrm{d}t_{ret}$, which gives us

$$\frac{\mathrm{d}W}{\mathrm{d}\Omega} = \left(\vec{S}\cdot\vec{n}(\vec{r},t')\right) R^2(\vec{r},t') \left(\frac{\mathrm{d}t}{\mathrm{d}t'}\right)\Big|_{t'=t_{ret}}. \tag{1.39}$$

From the definition of $t_{ret} \coloneqq t' - \frac{|\vec{r}-\vec{r}\,'|}{c}$ we find

$$\left(\frac{\mathrm{d}t}{\mathrm{d}t'}\right)\Big|_{t'=t_{ret}} = \left(1+\frac{1}{c}\frac{\mathrm{d}}{\mathrm{d}t'}|\vec{r}-\vec{r}_p(t')|\right)\Big|_{t'=t_{ret}} = \left(1-\frac{1}{c}\vec{n}(\vec{r},t')\vec{v}(t')\right)\Big|_{t'=t_{ret}}. \tag{1.40}$$

Finally we obtain

$$\frac{\mathrm{d}W}{\mathrm{d}\Omega} = \frac{q^2}{16\pi^2\epsilon_0 c}\frac{\left[\vec{n}(\vec{r},t')\times\left(\vec{n}(\vec{r},t')-\vec{\beta}(t')\right)\times\dot{\vec{\beta}}(t')\right]^2}{\left(1-\vec{\beta}(t')\cdot\vec{n}(\vec{r},t')\right)^5}\Bigg|_{t'=t_{ret}}. \tag{1.41}$$

Now we can discuss two cases. The non relativistic case ($\beta \approx 0$) and the relativistic case ($\beta \approx 1$).

$\beta \approx 0$: In this case (1.41) simplifies to

$$\begin{aligned}
\frac{\mathrm{d}W}{\mathrm{d}\Omega} &= \frac{q^2}{16\pi^2\epsilon_0 c}\left[\vec{n}(\vec{r},t')\times\left(\vec{n}(\vec{r},t')\times\dot{\vec{\beta}}(t')\right)\right]^2\Bigg|_{t'=t_{ret}} \\
&= \frac{q^2}{16\pi^2\epsilon_0 c}\left[\underbrace{\left(\vec{n}(\vec{r},t')\cdot\dot{\vec{\beta}}(t')\right)}_{=\dot{\beta}n\cos(\vartheta)}\vec{n}(\vec{r},t') - \underbrace{\left(\vec{n}(\vec{r},t')\cdot\vec{n}(\vec{r},t')\right)}_{|\cdot|=1}\dot{\vec{\beta}}(t')\right]^2\Bigg|_{t'=t_{ret}} \\
&= \frac{q^2\dot{\beta}_{ret}^2}{16\pi^2\epsilon_0 c}\left(\cos^2(\vartheta)-2\cos^2(\vartheta)+1\right) \\
&= \frac{q^2\dot{\beta}_{ret}^2}{16\pi^2\epsilon_0 c}\sin^2(\vartheta),
\end{aligned}$$

where ϑ is the angle between $\dot{\vec{\beta}}$ and $\vec{n}$. β_{ret} means again the evaluation at $t' = t_{ret}$. We conclude, that the direction of maximum radiation is perpendicular to the particles direction of motion, in contrast to

$\beta \approx 1$: where we will see shortly, that the maximum radiation will be primarily in the direction of motion of the particle. We will restrict ourselves to the simple case, where $\dot{\vec{\beta}} \parallel \vec{\beta}$. Following the same steps as above we obtain

$$\frac{\mathrm{d}W}{\mathrm{d}\Omega} = \frac{q^2 \dot{\beta}_{ret}^2}{16\pi^2 \epsilon_0 c} \frac{\sin^2(\vartheta)}{(1 - \beta(t')\cos(\vartheta))^5}. \tag{1.42}$$

The get the angle, where the radiation is maximal, we calculate

$$\begin{aligned}
&\frac{\mathrm{d}}{\mathrm{d}(\cos(\vartheta))}\left(\frac{\mathrm{d}W}{\mathrm{d}\Omega}\right) \overset{!}{=} 0 \\
&\iff -2\cos(\vartheta)\,(1 - \beta_{ret}\cos(\vartheta))^5 + 5\beta_{ret}(1 - \cos^2(\vartheta))\,(1 - \beta_{ret}\cos(\vartheta))^4 \overset{!}{=} 0 \\
&\iff (1 - \beta_{ret}\cos(\vartheta))^4 \left[-2\cos(\vartheta)\,(1 - \beta_{ret}\cos(\vartheta)) + 5\beta_{ret}(1 - \cos^2(\vartheta))\right] \overset{!}{=} 0 \\
&\implies -2\cos(\vartheta)\,(1 - \beta_{ret}\cos(\vartheta)) + 5\beta_{ret}(1 - \cos^2(\vartheta)) \overset{!}{=} 0 \\
&\iff \cos^2(\vartheta) + \frac{2}{3\beta_{ret}}\cos(\vartheta) - \frac{5}{3} \overset{!}{=} 0 \\
&\implies \cos(\vartheta)_{max} = \frac{1}{3\beta_{ret}}\left(\sqrt{1 + 15\beta_{ret}^2} - 1\right).
\end{aligned}$$

Obviously the angle decreases monotonically with increasing velocity, i.e. increasing β_{ret}. For $\beta_{ret} = 1$ we get $\cos(\vartheta) = 1$ or equivalently $\vartheta = 0$. In figure 1.2 the results are summarized.

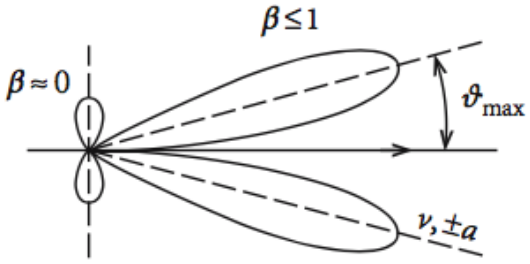

Figure 1.2.: Radiation characteristics of an moving charged particle.[6]

Part II.

Numerics

The following section deals with the numeric aspects of this thesis. We explain the underlying equation of motions and their history. After that, we go into several methods with which we can solve differential equations. Over the course of the last decades numerous methods were invented each of which has its own strength and weaknesses. Some of them are very easy to implement, which in turn usually leads to unprecise results. Others are quite complicated and sophisticated to implement, but very accurate. Therefore one should always consider which method is best for the problem and what it is one want to achieve.
Following this, we also want to define and calculate the numerical complexity of some chosen algorithms.

2

Integration of Equation of Motion

2.1 Equations of Motion

As we know from mechanics the dynamic of a particle is determined by the forces acting on it. In our case there is a force due to electro-magnetic fields. That can be external fields, but also fields due to moving particles, as we explained in section 1.3.
The dynamics of our system is described by the *Lorentz-Newton* equation

$$\begin{aligned} \frac{\mathrm{d}x^\mu}{\mathrm{d}\tau} &= u^\mu \\ \frac{\mathrm{d}u^\mu}{\mathrm{d}\tau} &= F^\mu_{\ \nu}\, u^\nu + g^\mu, \end{aligned} \tag{2.1}$$

which derivation is quite longish, why we want to refer to literature.
The term $F^\mu_{\ \nu}$ describes the electromagnetic field strength tensor

$$F^\mu_{\ \nu} = \begin{pmatrix} 0 & E_x & E_y & E_z \\ E_x & 0 & B_z & -B_y \\ E_y & -B_z & 0 & B_x \\ E_z & B_y & -B_x & 0 \end{pmatrix}. \tag{2.2}$$

The damping term g^μ considers the fact that charged particles radiate fields when they are moving which leads to a loss in their kinetic energy. Within the context of classical electrodynamics Max *Abraham* and Hendrick *Lorentz* discussed radiation damping in their same-named equation first. In 1938 *Dirac* generalized the equation whilst taking special relativity into account.
We now want to deal with how to solve the Lorentz-Newton equation (2.1) numerically.

2.2 Euler-Scheme

The most simple method is the explicit *Euler*-Method. It's easy to implement but not very accurate, as we shall see later. But before we go into the details of the explicit Euler-Scheme we need to address some prerequisites all following methods will have in

common.
Starting point will always be a first order system of the kind

$$\begin{aligned} \frac{\mathrm{d}x^\mu}{\mathrm{d}\tau} &= u^\mu \\ \frac{\mathrm{d}u^\mu}{\mathrm{d}\tau} &= f^\mu(x^\nu, u^\nu) \\ x^\mu(\tau_0) &= x_0^\mu \\ u^\mu(\tau_0) &= u_0^\mu. \end{aligned} \tag{2.3}$$

Systems of higher order can always be reduced to a first order system.
In order to solve the equation of motion numerically the domain needs to be discretized. Therefore we divide the time interval into N equidistant partial intervals h, by defining

$$h := \Delta\tau = \tau_{i+1} - \tau_i.$$

The idea is to calculate each point along the trajectory $x_i^\mu = x^\mu(\tau_i)$ iteratively, starting from the initial values x_0^μ and u_0^μ. But to calculate these points all differential operators in (2.3) need to be discretized as well. That is where all methods differ. Each method has its own way to discretize the differential operators.
The basis of the Euler-Scheme is a first order Taylor expansion of the integration variable x^μ in τ around τ_i

$$x^\mu(\tau_{i+1}) = x^\mu(\tau_i) + \frac{\mathrm{d}x^\mu}{\mathrm{d}\tau}\Big|_{\tau=\tau_i} \underbrace{(\tau_{i+1} - \tau_i)}_{=h} + \mathcal{O}(h^2). \tag{2.4}$$

Analogously for u^μ and solving for $\frac{\mathrm{d}x^\mu}{\mathrm{d}\tau}$ and $\frac{\mathrm{d}u^\mu}{\mathrm{d}\tau}$ respectively yields

$$\begin{aligned} \frac{x_{i+1}^\mu - x_i^\mu}{h} &= u_i^\mu \\ \frac{u_{i+1}^\mu - u_i^\mu}{h} &= f^\mu(x_i^\nu, u_i^\nu). \end{aligned} \tag{2.5}$$

This way of discretizing allows a very easy calculation of x_i^μ according to

$$\begin{aligned} x_{i+1}^\mu &= x_i^\mu + h\ u_i^\mu \\ u_{i+1}^\mu &= u_i^\mu + h\ f^\mu(x_i^\nu, u_i^\nu). \end{aligned} \tag{2.6}$$

In order for us to calculate the goodness of this approximation we need to introduce the *Procedural Error* and the *Order of Consistency*.[5]

2.2.1 Procedural Error and Order of Consistency

Definition 2.2.1 (Procedural Error and Order of Consistency) *Let $I \subseteq \mathbb{R}$ be a interval, $f : I \times \mathbb{R}^d \to \mathbb{R}^d$, $y : I \to \mathbb{R}^d$ a solution of the initial value problem*

$$\begin{aligned} \frac{\mathrm{d}}{\mathrm{d}\tau} y(\tau) &= f(\tau, y(\tau)), \\ y(\tau_0) &= y_0. \end{aligned} \tag{2.7}$$

(a) *The term*

$$\eta(\tau, h) := y(\tau) + h f(\tau, y(\tau)) - y(\tau + h) \quad \text{for } \tau \in I,\ 0 < h \leq b - \tau \tag{2.8}$$

is called local Procedural Error of the One-Step-Scheme at τ for the increment h.

(b) *The One-Step-Scheme has an Order of Consistency $p \geq 1$, if the local Procedural Error fulfils*

$$||\eta(\tau, h)|| \leq C h^{p+1} \quad \text{for } \tau \in I,\ 0 < h \leq b - \tau, \tag{2.9}$$

with a constant $C \geq 0$, which is independent of τ and h.

Descriptively the Procedural Error is the difference between the exact solution $y(\tau + h)$ and the result, which we get from the One-Step-Scheme starting from the exact solution at the earlier time step $y(\tau)$. Figure 2.1 illustrates the situation.

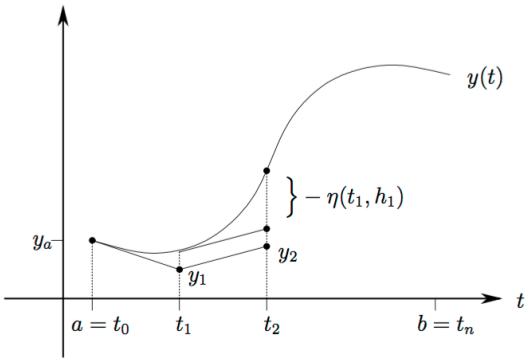

Figure 2.1.: Illustration of the Procedural Errors of an One-Step-Scheme. [5]

We now want to use the definitions 2.2.1 to calculate the Order of Consistency of the Euler-Scheme.
Starting point is the system (2.1). Thereby we focus on the equation for u^μ, since x^μ can be easily integrated from u^μ. Following Definition 2.2.1 we have

$$y = u^\mu. \tag{2.10}$$

We get

$$\eta(\tau, h) = u^\mu(\tau_i) + h f^\mu(x^\nu, u^\nu) - u^\mu(\tau_{i+1}). \tag{2.11}$$

The last term can be calculated with a Taylor-expansion analogously to (2.4).

$$u^\mu(\tau_{i+1}) = u^\mu(\tau_i) + h \left.\frac{\mathrm{d}u^\mu}{\mathrm{d}\tau}\right|_{s=\tau_i} + h^2 \left.\frac{\mathrm{d}^2u^\mu}{\mathrm{d}\tau^2}\right|_{s=\tau_i}. \tag{2.12}$$

Plugging in (2.12) in (2.11) yields

$$\begin{aligned} &\eta(\tau, h) = u^\mu(\tau_i) + h\frac{\mathrm{d}u^\mu}{\mathrm{d}\tau} - u^\mu(\tau_{i+1}) \\ \overset{(2.12)}{\Longrightarrow} &\eta(\tau, h) = u^\mu(\tau_i) + h\frac{\mathrm{d}u^\mu}{\mathrm{d}\tau} - u^\mu(\tau_i) - h\frac{\mathrm{d}u^\mu}{\mathrm{d}\tau} - h^2\frac{\mathrm{d}^2u^\mu}{\mathrm{d}\tau^2} \\ \Longleftrightarrow &\eta(\tau, h) = \frac{\mathrm{d}^2u^\mu}{\mathrm{d}\tau^2}\, h^2, \end{aligned} \tag{2.13}$$

since $\frac{\mathrm{d}u^\mu}{\mathrm{d}\tau} = f^\mu(x^\nu, u^\nu)$ holds for the Euler-Scheme. Thus

$$|\eta(\tau, h)| \leq Ch^2 \quad \text{with } C \coloneqq \frac{1}{2} \max_{\tau \in \mathcal{D}(u^\mu)} \left|\frac{\mathrm{d}^2u^\mu}{\mathrm{d}\tau^2}\right|. \tag{2.14}$$

$\mathcal{D}(u^\mu)$ denotes the domain of u^μ. Therefore, the Euler-Scheme has an Order of Consistency of one.

2.3 Leap-Frog-Scheme

A definitely better method is the so called *Leap-Frog*-Scheme. One can easily proof that it has an Order of Consistency of two.
In contrast to the explicit Euler-Scheme this method has several advantages. For one it is time reversible, i.e. it is possible to reach any previous point in time from every point later in the trajectory. On the other hand the Leap-Frog-Scheme is symplectic, meaning

it conserves the phase space volume from which energy and momentum conservation follows.
However, one disadvantage is that it's only suited for systems in which the acting force exclusively depends on the current position, but not on the velocity of the particle. This would lead to an implicit equation system which is numerically way more expensive to solve.
Thus the differential equation should be of the form

$$\frac{\mathrm{d}^2 x^\mu}{\mathrm{d}\tau^2} = \frac{\mathrm{d}u^\mu}{\mathrm{d}\tau} = f^\mu(x^\nu). \tag{2.15}$$

As we already mentioned, the various methods discretize the differential operators differently. The Leap-Frog-Scheme uses

$$\begin{aligned} \frac{x^\mu_{i+1} - x^\mu_i}{h} &= u^\mu_{i+\frac{1}{2}} \\ \frac{u^\mu_{i+\frac{1}{2}} - u^\mu_{i-\frac{1}{2}}}{h} &= f^\mu(x^\nu_i). \end{aligned} \tag{2.16}$$

Solving for the new time step yields

$$\begin{aligned} x^\mu_{i+1} &= x^\mu_i + h u^\mu_{i+\frac{1}{2}} \\ u^\mu_{i+\frac{1}{2}} &= u^\mu_{i-\frac{1}{2}} + h f^\mu(x^\nu_i). \end{aligned} \tag{2.17}$$

As we can see, position and velocity are calculated at different times. They are shifted against each other in time by $h = \frac{1}{2}$.
But what if we have a system in which the force depends on the velocity ? Are we stuck with expensive implicit methods ? Fortunately not. We can use the *Boris* - Method.

2.3.1 Boris-Method

This method was invented in 1970 by J.P. Boris[2] and is the standard method for pushing particles in plasma simulations today. We want to solve the Lorentz-Newton equation

$$\frac{v_{i+\frac{1}{2}} - v_{i-\frac{1}{2}}}{h} = \frac{q}{m}\left(\vec{E} + \frac{v_{i+\frac{1}{2}} + v_{i-\frac{1}{2}}}{2} \times \vec{B}\right) \tag{2.18}$$

Boris noticed, that upon defining

$$\begin{aligned} \vec{v}_- &:= v_{i-\frac{1}{2}} + \frac{h}{2}\frac{q\vec{E}}{m} \quad \text{and} \\ \vec{v}_+ &:= v_{i+\frac{1}{2}} + \frac{h}{2}\frac{q\vec{E}}{m}, \end{aligned} \tag{2.19}$$

one can eliminate the electric field. Plugging in (2.19) into (2.18) yields

$$\begin{aligned} \frac{\vec{v}_+ - \vec{v}_-}{h} &= \frac{q}{m}(\vec{v}_+ + \vec{v}_-) \times \vec{B} \\ \Longrightarrow |\vec{v}_+ - \vec{v}_-| &= \frac{qh}{m}|\vec{v}_+ + \vec{v}_-|B\underbrace{\sin(\vartheta)}_{=1}, \end{aligned} \tag{2.20}$$

where ϑ is the angle between $\vec{B}$ and $\vec{v}$. By splitting up the accelerating effect of the electric field in two parts with the rotational effect of the magnetic field in between, the accuracy is increased without having computational overhead. Hence, the steps are

1. Obtain $\vec{v}_-$ by starting from $v_{i-\frac{1}{2}}$ and adding half electric impulse.
2. Use rotation in (2.20) to obtain $\vec{v}_+$ and finally
3. obtain $v_{i+\frac{1}{2}}$ by adding yet another half electric impulse.

In Code we use the slightly more sophisticated but relativistically correct form with $u = \gamma v$.
Up to now one question remains unanswered. How do we solve for $\vec{v}_+$ in (2.20)? To answer this, we use figure 2.2.

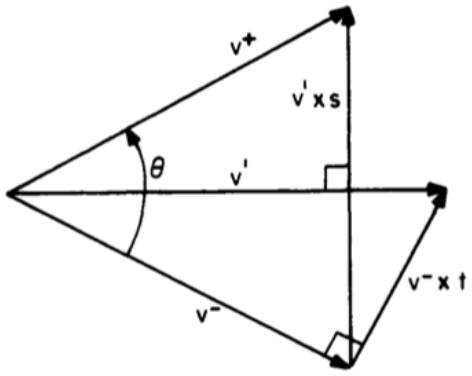

Figure 2.2.: Velocity space showing the rotation from $\vec{v}_-$ to $\vec{v}\,'$. The velocities shown are projections of the total velocities onto the plane perpendicular to $\vec{B}$. [3]

What we want is a vector, which is parallel to $\vec{v}_+ - \vec{v}_-$. Its magnitude is yet to be determined. However, if we can find a vector $\vec{v}\,'$ which is perpendicular to $\vec{v}_+ - \vec{v}_-$, then

$\vec{v}\,' \times \vec{s}$, where $\vec{s} \propto \vec{B}$, is exactly what we need.
Upon defining

$$\vec{t} \coloneqq -\frac{\vec{B}}{B} \tan\left(\frac{\theta}{2}\right) = \frac{q\vec{B}h}{2m}, \tag{2.21}$$

we obtain $\vec{v}\,'$ from

$$\vec{v}\,' = \vec{v}_- + \vec{v}_- \times \vec{t}. \tag{2.22}$$

Now $\vec{v}\,'$ is perpendicular to $\vec{v}_+ - \vec{v}_-$. Finally we need a vector $\vec{s} \propto \vec{B}$ wich magnitude is determined by the constraint $|\vec{v}_+| = |\vec{v}_-|$. Using half angle formulas we find

$$\vec{s} = \frac{2\vec{t}}{1+t^2}. \tag{2.23}$$

Hence

$$\vec{v}_+ = \vec{v}_- + \vec{v}\,' \times \vec{s}. \tag{2.24}$$

Finally we want to do a quick error analysis. We expect the angle of rotation θ to be close to

$$\omega_c h = \frac{2\pi h}{T} = \frac{qBh}{m},$$

where T is the period.
Following the geometrical analysis in [3] illustrated in 2.3 and using (2.20) we find

$$\begin{aligned} \left|\tan\left(\frac{\theta}{2}\right)\right| &= \frac{\frac{1}{2}|\vec{v}_+ - \vec{v}_-|}{\frac{1}{2}|\vec{v}_+ + \vec{v}_-|} = \frac{qB}{m}\frac{h}{2} = \frac{\omega_c h}{2} \\ \implies \theta &= 2\arctan\left(\frac{\omega_c h}{2}\right) = \omega_c h\left(1 - \frac{\omega_c^2 h^2}{12} + \dots\right). \end{aligned} \tag{2.25}$$

For $\omega_c h < 0.35$ we get an error smaller than 1%.

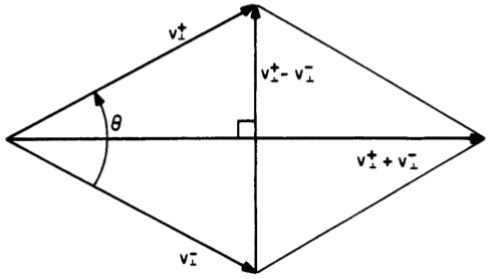

Figure 2.3.: Determination of $\left|\tan\left(\frac{\theta}{2}\right)\right|$ from boris rotation[3]

2.4 Nyström-Scheme

2.5 Adaptive Timestep Control

3

Interpolations

3.1 Linear interpolation of Trajectories

The previously presented methods calculate the particle trajectory solely at discrete points in time $x_i^\mu(\tau)$. Calculating Liénard-Wiechert fields according to equation (1.32) however, requires the intersection point of the trajectory with the backward lightcone of the observation point. In most cases the calculated points of the trajectory are not lying directly on the lightcone, so we need a procedure to calculate the intersection point exactly.
The simplest solution is a linear interpolation between the last point inside and the first point outside the lightcone. Figure 3.1 illustrates the situation.

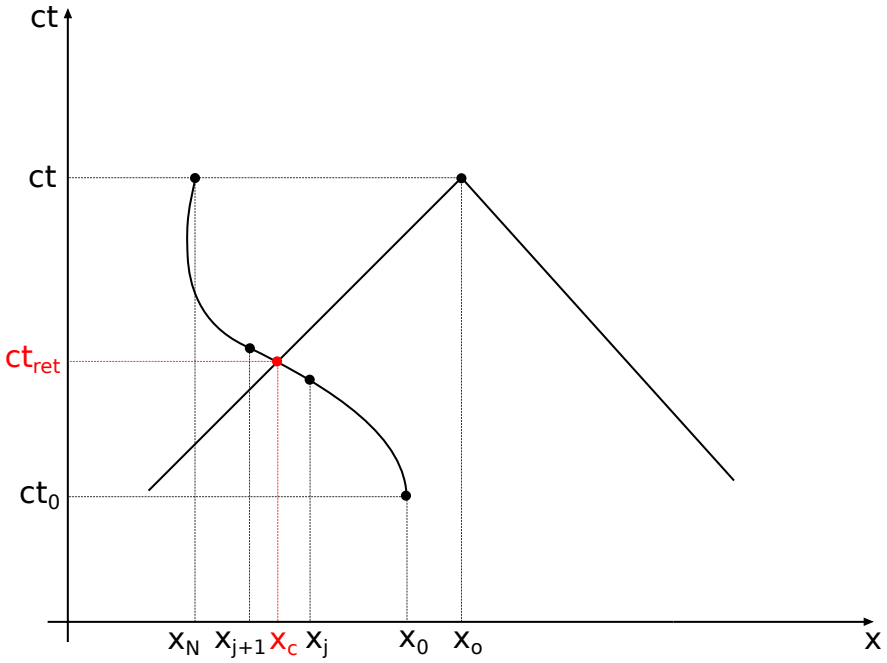

Figure 3.1.: Minkowski space showing the particle trajectory with starting point $x_0^\mu(t_0)$ and last point $x_N^\mu(t)$. The observation point $x_o^\mu(t)$ with its backward lightcone is also shown. If we want to calculate the Liénard-Wiechert fields at the observation point $x_o^\mu(t)$, we need the intersection point $x_c^\mu(t_{ret})$ of the trajectory with the backward lightcone.

Thereto let $x_j^\mu \in \mathbb{R}^{3+1}$ be the last point inside and $x_{j+1}^\mu \in \mathbb{R}^{3+1}$ the first point outside the lightcone. Further let $x_c^\mu \in \mathbb{R}^{3+1}$ be the intersection point of interest then we get

$$x_c^\mu = x_j^\mu + \lambda \left(x_{j+1}^\mu - x_j^\mu \right), \tag{3.1}$$

where $\lambda \in [0, 1]$. Due to the finite speed of light the intersection point x_c^μ needs to fulfill

$$|\vec{x}_o(t) - \vec{x}_c(t_{ret})| = c\ (t - t_{ret}) \Longleftrightarrow (x_o - x_c)_\mu (x_o - x_c)^\mu = 0. \tag{3.2}$$

Thereby $x_o^\mu \in \mathbb{R}^{3+1}$ denotes the observation point where the fields shall be calculated. Note, that on the left hand side of (3.2) only spatial components of the respective four vectors are used.
Plugging in (3.1) in (3.2) yields

$$\lambda^2(x_{j+1}-x_j)_\mu(x_{j+1}-x_j)^\mu + \lambda\, 2(x_{j+1}-x_j)_\mu(x_j-x_o)^\mu + (x_j)_\mu(x_j)^\mu \\ + (x_o)_\mu(x_o)^\mu - 2(x_j)_\mu(x_o)^\mu = 0. \quad (3.3)$$

We define

$$a \coloneqq (x_{j+1}-x_j)_\mu(x_{j+1}-x_j)^\mu$$
$$b \coloneqq 2(x_{j+1}-x_j)_\mu(x_j-x_o)^\mu$$
$$c \coloneqq (x_j)_\mu(x_j)^\mu + (x_o)_\mu(x_o)^\mu - 2(x_j)_\mu(x_o)^\mu.$$

In general the quadratic equation (3.3) in λ has two solutions

$$\lambda_{1/2} = \frac{-b \pm \sqrt{b^2-4ac}}{2a}.$$

One denotes the intersection point with the backward lightcone, the other one with the forward lightcone. Since $\lambda \in [0,1]$ we are only interested in the larger one.

$$\lambda_{1/2} = \frac{-b + \sqrt{b^2-4ac}}{2a}.$$

Plugging in λ in (3.1) gives the desired intersection point.

3.2 Trilinear Interpolation of Fields

Another interpolation method we are using is the trilinear interpolation to calculate the field values at the particle position more accurately. As is explained in more detail later (see chapter 5), field values will either be stored on grid points or calculated analytically. However, if we want to consider interactions between multiple particles correctly, we need the field values at the particle position which does usually not coincide with the grid point where the field values are stored. Matters were complicated further by the fact that our grid will be staggered, due to numerical stability issues and is explained in more detail in section 5.2.
So, let's assume we have a cube with the points A,B,C, ...,H, as is illustrated in the following figure 3.2

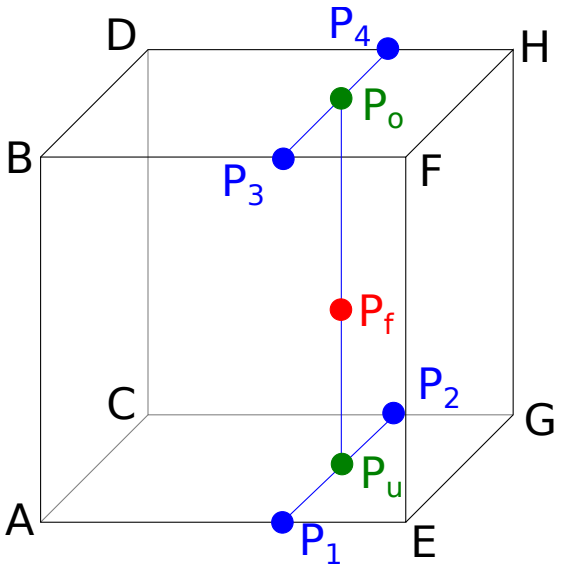

Figure 3.2.: Cube with its eight corner points and interpolation point P_f

Those eight points are part of the grid and contain the field values for both $\vec{E}$ and $\vec{H}$. To get the correct field values at the particle position P_f we need to interpolate in 3D. The trilinear interpolation simply consists out of seven linear interpolations. We first interpolate the x - value along AE, CG, BF and DH to get the points P_1, P_2, P_3 and P_4. Thereto let $x_p \in \mathbb{R}$ be the particle's x position and $x_0 \in \mathbb{R}$ and $x_1 \in \mathbb{R}$ be the corresponding x - values at A and E respectively. Same holds for the aforementioned tuples as well. Then we can write

$$\begin{aligned} u &:= \frac{x_p - x_0}{x_1 - x_0} \\ \implies P_1 &= A + u(E - A) \\ \implies P_2 &= C + u(G - C) \\ \implies P_3 &= B + u(F - B) \\ \implies P_4 &= D + u(H - D). \end{aligned} \tag{3.4}$$

In the next step, we interpolate along the y - axis. Analogously we define y_p, y_0 and y_1.

We conclude

$$\begin{aligned} v &:= \frac{y_p - y_0}{y_1 - y_0} \\ \implies P_u &= P_1 + v(P_2 - P_1) \\ \implies P_o &= P_3 + v(P_4 - P_3). \end{aligned} \tag{3.5}$$

And finally with z_p, z_0 and z_1 we get

$$\begin{aligned} w &:= \frac{z_p - z_0}{z_1 - z_0} \\ \implies P_f &= P_u + v(P_o - P_u). \end{aligned} \tag{3.6}$$

4

FDTD

In this section we introduce the concept of hybrid fields and how this approach reduces the numerical complexity from N^2 to N.
Usually the numerical complexity of multi particle simulation is N^2, due to the interaction between each particle. In our case we need N push operations for the particles. One push for each particle. In order to do that, however, we need to solve equation (2.1) and therefore all Liénard-Wiechert fields from the other $N-1$ particles are needed. This results in $N(N-1)$ calculations for each time step. If we want to calculate the Liénard-Wiechert fields, we also need to store all positions from all particles, as explained in section 3.1. For a few particles such simulations are effortlessly feasible. But with increasing particle numbers such simulations may not just require more and more memory capacity but also become so time consuming that at some point we simply can not do them anylonger. That's where the hybrid field model comes in. Instead of calculating the Liénard-Wiechert fields at every time step for all particles at all grid points we save them onto the grid and propagate them through the grid using Maxwell equations. How that works in detail is explained in the following sections.

4.1 The Yee-Scheme

In this section we talk about how to solve the Maxwell Equations (1.2) and how to propagate the fields on a numerical grid. We thereby focus on the Maxwell Equations in vacuum, i.e. $\rho = \vec{j} = 0$. As can be seen in the Liénard-Wiechert formula (1.32) there is a singularity for the field values at the particle position itself. Thus, we just want to propagate fields far away from the source, which is explained in more detail later.

To push the fields on the grid. i.e solving for the fields at the next time step, we use the Yee - Scheme introduced by *Kane Yee* in 1966[8] to discretize the Maxwell Equations. Each point on the discretized grid is represented as a tuple (i, j, k). One index for each dimension (x, y, z). The distance between the grid points are $(\Delta x, \Delta y, \Delta z)$ respectively. h denotes the time discretization as before. In order to have finite central differences rather than plain finite differences, the evaluation of $\vec{E}$ and $\vec{H}$ components are shifted in

time about $\frac{h}{2}$ against each other. To have the same benefits for the rotation, the $\vec{E}$ and $\vec{H}$ components are shifted in space as well, as it's illustrated in figure 4.1.

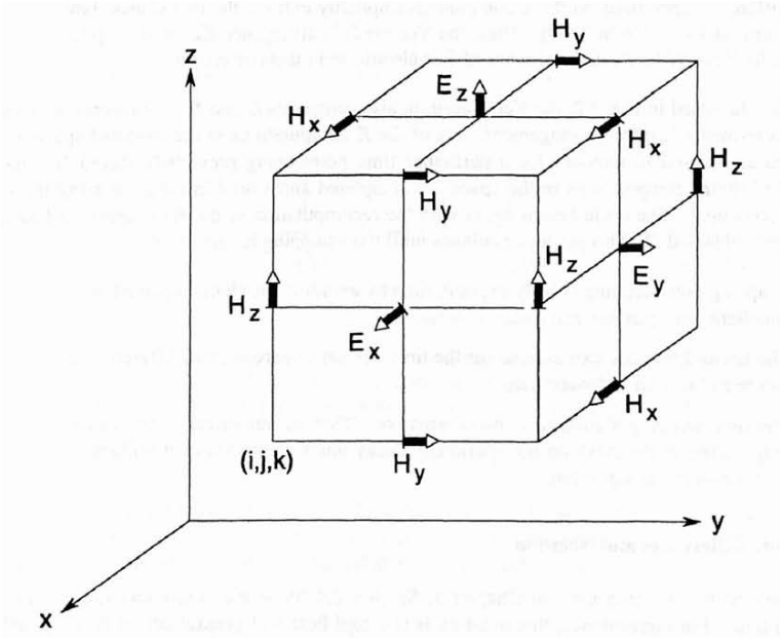

Figure 4.1.: An illustration of a so called Yee-Box which is used to solve the curl Maxwell Equations. Shown are the positions of the electric and magnetic field vector components about a cubic unit cell of the Yee space lattice.The Yee algorithm centers its E and H components in three- dimensional space so that every E component is surrounded by four circulating H components, and every H component is surrounded by four circulating E components.[7]

The discrete Maxwell equations then read

$$\begin{aligned} \frac{\vec{E}\Big|_{(i,j,k)}^{n+\frac{1}{2}} - \vec{E}\Big|_{(i,j,k)}^{n-\frac{1}{2}}}{h} &= \vec{\nabla}^{-} \times \vec{H}\Big|_{(i,j,k)}^{n}, \\ \frac{\vec{H}\Big|_{(i,j,k)}^{n+1} - \vec{H}\Big|_{(i,j,k)}^{n}}{h} &= \vec{\nabla}^{+} \times \vec{E}\Big|_{(i,j,k)}^{n+\frac{1}{2}}. \end{aligned} \tag{4.1}$$

The operators $\vec{\nabla}^-$ and $\vec{\nabla}^+$ act on a discretized vector field $F\Big|_{(i,j,k)} : \mathbb{R}^3 \to \mathbb{R}$ as follows

$$\vec{\nabla}^- F\Big|_{(i,j,k)} := \begin{pmatrix} \frac{F\Big|_{(i,j,k)} - F\Big|_{(i-1,j,k)}}{\Delta x}, \frac{F\Big|_{(i,j,k)} - F\Big|_{(i,j-1,k)}}{\Delta y}, \frac{F\Big|_{(i,j,k1)} - F\Big|_{(i,j,k-1)}}{\Delta z} \end{pmatrix}^T, \tag{4.2}$$

$$\vec{\nabla}^+ F\Big|_{(i,j,k)} := \begin{pmatrix} \frac{F\Big|_{(i+1,j,k)} - F\Big|_{(i,j,k)}}{\Delta x}, \frac{F\Big|_{(i,j+1,k)} - F\Big|_{(i,j,k)}}{\Delta y}, \frac{F\Big|_{(i,j,k+1)} - F\Big|_{(i,j,k)}}{\Delta z} \end{pmatrix}^T, \tag{4.3}$$

where T denotes the transpose as usual. The spatial positions where $\vec{E}$ and $\vec{H}$ components will be calculated are given by

$$\begin{aligned} \vec{E}\Big|_{(i,j,k)} &= \begin{pmatrix} E_x\left[\left(i+\frac{1}{2}\right)\Delta x, j\Delta y, k\Delta z\right] \\ E_y\left[i\Delta x, \left(j+\frac{1}{2}\right)\Delta y, k\Delta z\right] \\ E_z\left[i\Delta x, j\Delta y, \left(k+\frac{1}{2}\right)\Delta z\right] \end{pmatrix}, \\ \vec{H}\Big|_{(i,j,k)} &= \begin{pmatrix} H_x\left[i\Delta x, \left(j+\frac{1}{2}\right)\Delta y, \left(k+\frac{1}{2}\right)\Delta z\right] \\ H_y\left[\left(i+\frac{1}{2}\right)\Delta x, j\Delta y, \left(k+\frac{1}{2}\right)\Delta z\right] \\ H_z\left[\left(i+\frac{1}{2}\right)\Delta x, \left(j+\frac{1}{2}\right)\Delta y, \Delta z\right] \end{pmatrix}. \end{aligned} \tag{4.4}$$

4.2 Numeric Dispersion Relation

By discretizing the numerical grid, the dispersion relation of light also changes. To study this effect we need to solve the discretized Maxwell Equations (4.1). Without loss of generality we choose the Ansatz of a TMz-mode, i.e. $H_z = 0$ and $E_z \neq 0$:

$$\begin{aligned} E_z\Big|^n_{(i,j,k)} &= E_{z_0} \exp\left\{\hat{i}\left(\tilde{k}_x i\Delta x + \tilde{k}_y i\Delta y - \omega n h\right)\right\} \\ H_x\Big|^n_{(i,j,k)} &= H_{x_0} \exp\left\{\hat{i}\left(\tilde{k}_x i\Delta x + \tilde{k}_y i\Delta y - \omega n h\right)\right\} \\ H_y\Big|^n_{(i,j,k)} &= H_{y_0} \exp\left\{\hat{i}\left(\tilde{k}_x i\Delta x + \tilde{k}_y i\Delta y - \omega n h\right)\right\}, \end{aligned} \tag{4.5}$$

where $\hat{i}$ denotes the imaginary unit and $\tilde{k}_x$, $\tilde{k}_y$ the x- and y-components of the wave vector. Using TMz-mode, (4.1) also simplifies to

$$\begin{aligned}
\frac{E_z\Big|_{(i,j,k)}^{n+\frac{1}{2}} - E_z\Big|_{(i,j,k)}^{n-\frac{1}{2}}}{h} &= \left(\frac{H_y\Big|_{(i,j,k)}^{n} - H_y\Big|_{(i-1,j,k)}^{n}}{\Delta x} - \frac{H_x\Big|_{(i,j,k)}^{n} - H_x\Big|_{(i,j-1,k)}^{n}}{\Delta y} \right) \\
\frac{H_x\Big|_{(i,j,k)}^{n+1} - H_x\Big|_{(i,j,k)}^{n}}{h} &= -\left(\frac{E_z\Big|_{(i,j+1,k)}^{n+\frac{1}{2}} - E_z\Big|_{(i,j,k)}^{n+\frac{1}{2}}}{\Delta y} \right) \\
\frac{H_y\Big|_{(i,j,k)}^{n+1} - H_y\Big|_{(i,j,k)}^{n}}{h} &= \left(\frac{E_z\Big|_{(i+1,j,k)}^{n+\frac{1}{2}} - E_z\Big|_{(i,j,k)}^{n+\frac{1}{2}}}{\Delta x} \right).
\end{aligned} \tag{4.6}$$

Upon substituting (4.5) in (4.6) and after some manipulation we find

$$E_{z_0} \sin\left(\frac{\omega h}{2}\right) = h\left[\frac{H_{x_0}}{\Delta y}\sin\left(\frac{\tilde{k}_y \Delta y}{2}\right) - \frac{H_{y_0}}{\Delta x}\sin\left(\frac{\tilde{k}_x \Delta x}{2}\right)\right] \tag{4.7}$$

$$H_{x_0} = \frac{hE_{z_0}}{\Delta y}\frac{\sin\left(\frac{\tilde{k}_y \Delta y}{2}\right)}{\sin\left(\frac{\omega h}{2}\right)} \tag{4.8}$$

$$H_{y_0} = \frac{hE_{z_0}}{\Delta x}\frac{\sin\left(\frac{\tilde{k}_x \Delta x}{2}\right)}{\sin\left(\frac{\omega h}{2}\right)}. \tag{4.9}$$

Plugging in (4.8) and (4.9) in (4.6) we obtain the numerical dispersion relation

$$\left[\frac{1}{h}\sin\left(\frac{\omega h}{2}\right)\right]^2 = \left[\frac{1}{\Delta x}\sin\left(\frac{\tilde{k}_x \Delta x}{2}\right)\right]^2 + \left[\frac{1}{\Delta y}\sin\left(\frac{\tilde{k}_y \Delta y}{2}\right)\right]^2 \tag{4.10}$$

For the one dimensional case (4.10) reduces to

$$\omega h = 2\arcsin\left(\frac{\Delta t}{\Delta x}\sin\left(\frac{\tilde{k}_x \Delta x}{2}\right)\right), \tag{4.11}$$

which is still more complicated than the analytic dispersion relation

$$\omega = k. \tag{4.12}$$

In figure 4.2 both the analytical and the numerical dispersion relation are plotted. Equation (4.11) has a maximum at

$$\begin{aligned} \tilde{k}_x^{max} &= \frac{\pi}{\Delta x} \\ \iff \lambda_x^{max} &= 2\Delta x. \end{aligned} \tag{4.13}$$

$\tilde{k}_x^{max}$ is the largest possible wavevector - also called *Nyquist Limit* for a numerical grid with resolution Δx, or Δy, Δz respectively. At this wavevector, the group velocity

$$v_g = \frac{\partial \tilde{k}_x}{\partial \omega}\Big|_{\tilde{k}=\tilde{k}^{max}} = 0. \tag{4.14}$$

vanishes, instead of propagating with speed of light. That means, that the Yee-Scheme is only valid for wavelength $\lambda \ll \lambda^{max}$.

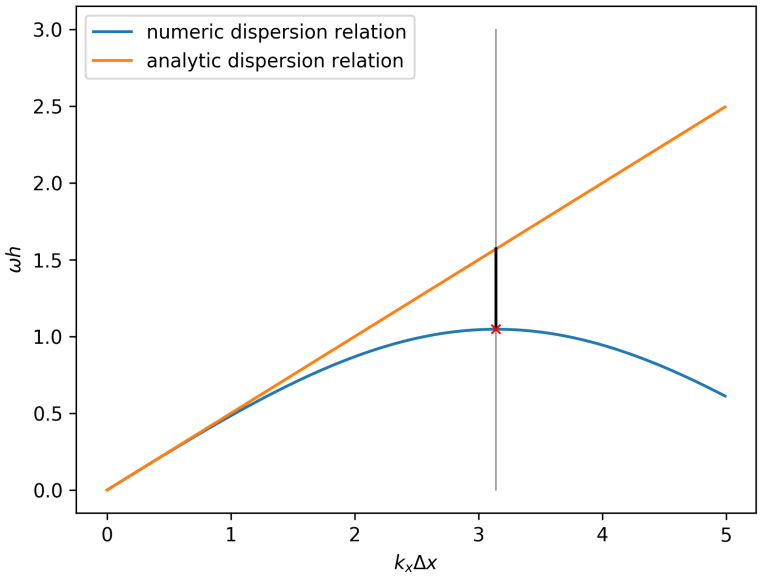

Figure 4.2.: Comparison of numerical and analytical dispersion relation of discretized Maxwell Equations with Yee Scheme. We used $c \equiv 1$ and $\frac{\Delta t}{\Delta x} \equiv \frac{1}{2}$.

5

Hybrid Field Approach

After having discussed the fundamentals, we now want to dive into practice. In section 5.2 we learned how to store and propagate the fields on a numerical grid. In section 1.3 we derived an analytical expression, of how to calculate the fields of a moving charged particle. We also observed that there is a singularity in (1.32) at the particle position itself. That means, that the fields will vary strongly in a vicinity of the particle and can not be resolved correctly on the grid, as discussed in section 4.2. Hence, it seems plausible to separate the simulation area into appropriate Near - and Farfield areas. Within the Nearfield area of a particle, its fields will **not** be stored on the grid. We then do not need to worry about the singularity. Only Farfields from other particles, propagated into the Nearfield area will be further propagated and stored on the grid. Possible interactions with other particles within the Nearfield area will be caluclated analytically from (1.32). Farfields will be stored on the grid and propagated with the Yee-Scheme (4.1).

5.1 Near-and Farfields

Before we can separate the simulation area into Near - and Farfields, we need to initialize a grid. We divide the grid in `numberBoxesInX`, `numberBoxesInY` and `numberBoxesInZ` boxes, each of which has `numberOfGridPointsForBoxInX`, `numberOfGridPointsForBoxInY` and `numberOfGridPointsForBoxInZ` length, which leaves us with a total

```
numberOfGridPointsInX = numberOfGridPointsForBoxInX * numberOfBoxesInX;
numberOfGridPointsInY = numberOfGridPointsForBoxInY * numberOfBoxesInY;
numberOfGridPointsInZ = numberOfGridPointsForBoxInZ * numberOfBoxesInZ;
```

Upon defining the resolution `dx`, `dy`, `dz` the size of the simulation area is then given by

```
lengthOfSimulationBoxInX = numberOfGridPointsInX * dx;
lengthOfSimulationBoxInY = numberOfGridPointsInY * dy;
lengthOfSimulationBoxInZ = numberOfGridPointsInZ * dz;
```

The Nearfield is then defined as the $3 \cdot 3 \cdot 3 = 27$ boxes with the box, containing the particle, in the center. In figure 5.1 the Nearfields of one and two particles are shown.

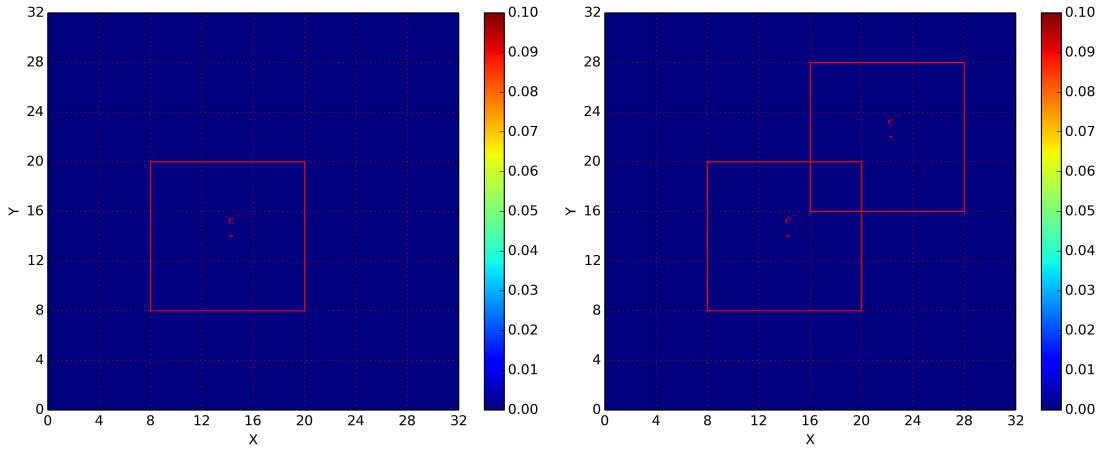

(a) (b)

Figure 5.1.: Nearfields of one (a) and two (b) particles. The box at $(18, 18)$ belongs to the Nearfield of both particles, marked with e^-. Notice the staggered red grid in the background. In this example we used 8 boxes, with 20 grid points each, and a resolution of $dx = dy = dz = 0.2$. The plotted plane was chosen accordingly to the z - coordinate of the particle.

The Nearfields can of course overlap. The Nearfield box at $(18, 18)$ belongs to both particles.

5.2 Field Push

We now want to explain, how a field push actually works. Since we only propagate fields in the Farfield area as explained in section special care needs to be taken at the boundaries between Farfield and Nearfield. To explain this, consider the following plane of a grid illustrated in figure 5.2

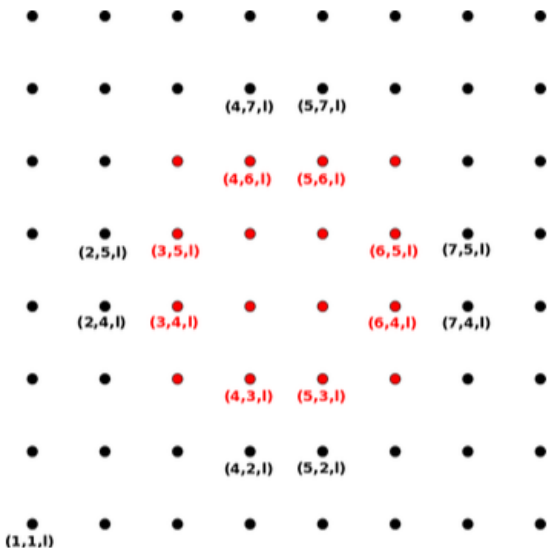

Figure 5.2.: One plane of a grid showing the Nearfield and Farfield of a particle. The Nearfield does not contain any field values of the particle.[4]

The red dots are considered to be the Nearfield area of a particle. The black dots are therefore the Farfield area. The grid points within the Nearfild does not contain any field values. We only store and propagate fields on the grid points in the Farfield. If we now want to push the value for H_z at $(2, 4, k)$ (recall that each grid point contains the field values for either H_x, H_y, H_z or E_x, E_y, E_z due to the staggered grid, explained in section 5.2), where $k \in (1, 2, 3, \ldots, \text{numberOfGridPointsInZ} - 1)$, we need to solve

$$\frac{\partial H_z}{\partial t} = -\left(\frac{\partial E_y}{\partial x} - \frac{\partial E_x}{\partial y}\right). \tag{5.1}$$

Using the discretized Maxwell Equations (4.1) we get

$$\vec{H}\Big|_{z(2,4,k)}^{n+1} = \vec{H}\Big|_{z(2,4,k)}^{n} - h\left(\frac{E\Big|_{y(3,4,k)}^{n+\frac{1}{2}} - E\Big|_{y(2,4,k)}^{n+\frac{1}{2}}}{\Delta x} - \frac{E\Big|_{x(2,5,k)}^{n+\frac{1}{2}} - E\Big|_{y(2,4,k)}^{n+\frac{1}{2}}}{\Delta y}\right). \tag{5.2}$$

$\vec{H}\Big|_{z(2,4,k)}^{n+1}$ is stored on a Farfield grid point. Its calculation, however, requires a field value

$E\big|^{n+\frac{1}{2}}_{y(3,4,k)}$, which is stored on a Nearfield grid point and therefore contains no field values from the particle (it can however contain field values from other particles propagated from the outside into the Nearfield area). Hence we need to analytically calculate the Liénard-Wiechert field (1.32) of the particle at $(3,4,k)$ $E\big|^{n+\frac{1}{2}}_{yp(3,4,k)}$ and add it to the field value already stored at this grid point. Finally the correct calculation is

$$\vec{H}\Big|^{n+1}_{z(2,4,k)} = \vec{H}\Big|^{n}_{z(2,4,k)} - h\left(\frac{\left(E\big|^{n+\frac{1}{2}}_{y(3,4,k)} + E\big|^{n+\frac{1}{2}}_{yp(3,4,k)}\right) - E\big|^{n+\frac{1}{2}}_{y(2,4,k)}}{\Delta x} - \frac{E\big|^{n+\frac{1}{2}}_{x(2,5,k)} - E\big|^{n+\frac{1}{2}}_{y(2,4,k)}}{\Delta y}\right) \tag{5.3}$$

On the contrary, if we want to push the value for H_z at $(6,4,k)$ we need to analytically calculate the Liénard-Wiechert field (1.32) of the particle at $(7,4,k)$ $E\big|^{n+\frac{1}{2}}_{yp(7,4,k)}$ and subtract it from the field value already stored at this grid point. $(7,4,k)$ already contains the field contribution of the particle, since it is a Farfield grid point. And because $(6,4,k)$ is a Nearfield grid point we only want to take contributions from other particles into account, which are about to propagate into our Nearfield area. After subtracting our own contributions the correct push can be calculated via

$$\vec{H}\Big|^{n+1}_{z(6,4,k)} = \vec{H}\Big|^{n}_{z(6,4,k)} - h\left(\frac{\left(E\big|^{n+\frac{1}{2}}_{y(7,4,k)} - E\big|^{n+\frac{1}{2}}_{yp(7,4,k)}\right) - E\big|^{n+\frac{1}{2}}_{y(6,4,k)}}{\Delta x} - \frac{E\big|^{n+\frac{1}{2}}_{x(6,5,k)} - E\big|^{n+\frac{1}{2}}_{y(6,4,k)}}{\Delta y}\right) \tag{5.4}$$

This and more examples as well as a more detailed explanation can be found in.[4] All points along the boarder between Near - and Farfield need to be adjusted accordingly.

We now want to explain how this works out in Code. Figure 5.3 shows three boxes, two of which are Nearfield boxes and one is a Farfield box. For reasons of clarity we only show the grid points along the edges.

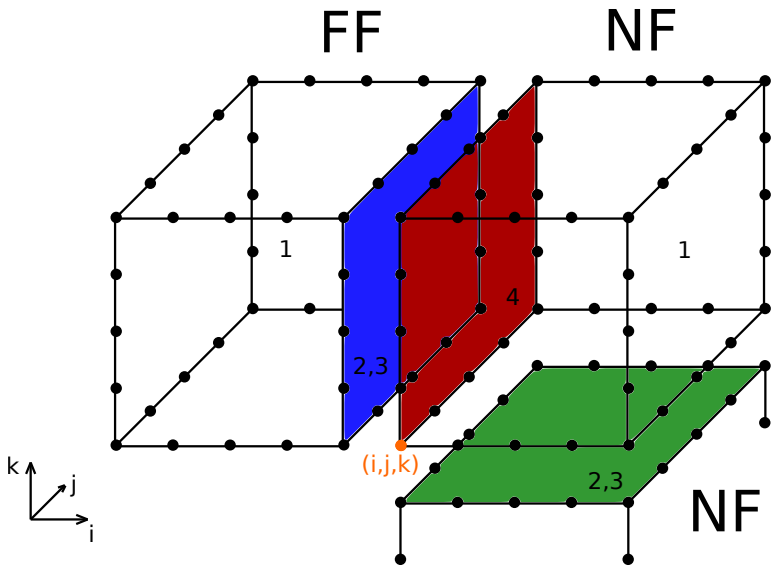

Figure 5.3.: Section of a grid with three boxes, two of which are Nearfield boxes (NF) and one being a Farfield box (FF). The colored planes represent those grid points, where adjustments are necessary, as explained above. One H - Field push consists of four steps. or equivalently four subroutines in Code: 1. `pushHFieldInsideBoxes`, 2. `setEFieldOnBoarders`, 3. `adjustEFields`, 4 `.pushHFieldAtBorders`. For reasons of clarity we left out the grid points within the boxes.

5.3 Particle Push and Nearfield Update

5.4 Particle History

5.5 Farfield Setup Before Simulation

5.6 Electron Scattering in an electromagnetic wave

6

Uniaxial Perfectly Matched Layer

Part III.

Summary

Part IV.

Appendix

A

Gauge Transformations

In this chapter we want to show, that the gauge fields leave both the electric and magnetic fields and the corresponding potential equations invariant.

A.1 Invariance of Fields

We want to show that $\vec{E}' = \vec{E}$ and $\vec{B}' = \vec{B}$.

$$\begin{aligned}
\vec{E}' &= -\vec{\nabla}\varphi' - \frac{\partial \vec{A}'}{\partial t} \\
&= -\vec{\nabla}\left(\varphi - \frac{\partial \psi}{\partial t}\right) - \frac{\partial}{\partial t}\left(\vec{A} + \vec{\nabla}\psi\right) \\
&= -\vec{\nabla}\varphi + \vec{\nabla}\left(\frac{\partial \psi}{\partial t}\right) - \frac{\partial \vec{A}}{\partial t} - \frac{\partial}{\partial t}(\vec{\nabla}\psi) \\
&= \vec{E}
\end{aligned}$$

and

$$\begin{aligned}
\vec{B}' &= \vec{\nabla} \times \vec{A}' \\
&= \vec{\nabla} \times \left(\vec{A} + \vec{\nabla}\psi\right) \\
&= \vec{\nabla} \times \vec{A} + \vec{\nabla} \times (\vec{\nabla}\psi) \\
&= \vec{B}.
\end{aligned}$$

A.2 Invariance of Potential Equations

Now we want to show the invariance of the potential equations. Therefore consider

$$\begin{aligned}
-\Delta\varphi' - \vec{\nabla}\left(\frac{\partial \vec{A}'}{\partial t}\right) &= \frac{\rho}{\epsilon_0} \\
\iff -\Delta\left(\varphi - \frac{\partial\psi}{\partial t}\right) - \vec{\nabla}\left[\frac{\partial}{\partial t}\left(\vec{A} + \vec{\nabla}\psi\right)\right] &= \frac{\rho}{\epsilon_0} \\
\iff -\Delta\varphi + \Delta\left(\frac{\partial\psi}{\partial t}\right) - \vec{\nabla}\left(\frac{\partial\vec{A}}{\partial t}\right) - \vec{\nabla}\left[\frac{\partial}{\partial t}\left(\vec{\nabla}\psi\right)\right] &= \frac{\rho}{\epsilon_0} \\
\iff -\Delta\varphi - \vec{\nabla}\left(\frac{\partial\vec{A}}{\partial t}\right) &= \frac{\rho}{\epsilon_0}
\end{aligned}$$

and

$$\begin{aligned}
\Box\vec{A}' - \vec{\nabla}\left(\vec{\nabla}\vec{A}' + \frac{1}{c^2}\frac{\partial\varphi'}{\partial t}\right) &= -\mu_0\vec{j} \\
\iff \hat{\Box}\left(\vec{A} + \vec{\nabla}\psi\right) - \vec{\nabla}\left[\vec{\nabla}\left(\vec{A} + \vec{\nabla}\psi\right) + \frac{1}{c^2}\frac{\partial}{\partial t}\left(\varphi - \frac{\partial\psi}{\partial t}\right)\right] &= -\mu_0\vec{j} \\
\iff \hat{\Box}\vec{A} + \Box\left(\vec{\nabla}\psi\right) - \vec{\nabla}\left[\vec{\nabla}\vec{A} + \Delta\psi + \frac{1}{c^2}\frac{\partial\varphi}{\partial t} - \frac{1}{c^2}\frac{\partial^2\psi}{\partial t^2}\right] &= -\mu_0\vec{j} \\
\iff \hat{\Box}\vec{A} + \Box\left(\vec{\nabla}\psi\right) - \vec{\nabla}\left[\vec{\nabla}\vec{A} + \Box\psi + \frac{1}{c^2}\frac{\partial\varphi}{\partial t}\right] &= -\mu_0\vec{j} \\
\iff \hat{\Box}\vec{A} - \vec{\nabla}\left(\vec{\nabla}\vec{A} + \frac{1}{c^2}\frac{\partial\varphi}{\partial t}\right) &= -\mu_0\vec{j}
\end{aligned}$$

B

Retarded Potential Equations Fulfill Laurentz Gauge

We show that the retarded potential equations

$$\begin{aligned}\varphi(\vec{r},t) &= \frac{1}{4\pi\epsilon_0}\int_V \frac{\rho(\vec{r}\,',t_{ret})}{|\vec{r}-\vec{r}\,'|}\mathrm{d}\vec{r}\,',\\ \vec{A}(\vec{r},t) &= \frac{\mu_0}{4\pi}\int_V \frac{\vec{j}(\vec{r}\,',t_{ret})}{|\vec{r}-\vec{r}\,'|}\mathrm{d}\vec{r}\,'\end{aligned}$$

with $t_{ret} \coloneqq t - \frac{|\vec{r}-\vec{r}\,'|}{c}$ fulfill the Laurentz Gauge

$$\vec{\nabla}\vec{A} + \frac{1}{c^2}\frac{\partial\varphi}{\partial t} = 0.$$

Plugging in yields

$$\begin{aligned}\vec{\nabla}\vec{A} + \frac{1}{c^2}\frac{\partial\varphi}{\partial t} &= \frac{\mu_0}{4\pi}\int_V \vec{\nabla}_{\vec{r}}\,\frac{\vec{j}(\vec{r}\,',t_{ret})}{|\vec{r}-\vec{r}\,'|}\mathrm{d}\vec{r}\,' + \frac{1}{c^2}\frac{1}{4\pi\epsilon_0}\int_V \frac{\partial}{\partial t}\frac{\rho(\vec{r}\,',t_{ret})}{|\vec{r}-\vec{r}\,'|}\mathrm{d}\vec{r}\,'\\ &= \frac{\mu_0}{4\pi}\int_V \vec{\nabla}_{\vec{r}}\,\frac{\vec{j}(\vec{r}\,',t_{ret})}{|\vec{r}-\vec{r}\,'|}\frac{\partial}{\partial t}\frac{\rho(\vec{r}\,',t_{ret})}{|\vec{r}-\vec{r}\,'|}\mathrm{d}\vec{r}\,',\end{aligned}$$

where we used $c^2 = \frac{1}{\mu_0\epsilon_0}$. Now consider the first term in the integrand

$$\begin{aligned}\vec{\nabla}_{\vec{r}}\,\frac{\vec{j}(\vec{r}\,',t_{ret})}{|\vec{r}-\vec{r}\,'|} &= \vec{j}(\vec{r}\,',t_{ret})\vec{\nabla}_{\vec{r}}\left(\frac{1}{|\vec{r}-\vec{r}\,'|}\right) + \frac{1}{|\vec{r}-\vec{r}\,'|}\partial_{t_{ret}}\vec{j}(\vec{r}\,',t_{ret})\vec{\nabla}_{\vec{r}}\,t_{ret}\\ &= -\vec{j}(\vec{r}\,',t_{ret})\frac{\vec{r}-\vec{r}\,'}{|\vec{r}-\vec{r}\,'|^3} - \frac{1}{c}\frac{\vec{r}-\vec{r}\,'}{|\vec{r}-\vec{r}\,'|^2}\partial_{t_{ret}}\vec{j}(\vec{r}\,',t_{ret})\end{aligned}$$

On the other hand we also have

$$\begin{aligned}\vec{\nabla}_{\vec{r}\,'}\,\frac{\vec{j}(\vec{r}\,',t_{ret})}{|\vec{r}-\vec{r}\,'|} &= \vec{j}(\vec{r}\,',t_{ret})\vec{\nabla}_{\vec{r}\,'}\left(\frac{1}{|\vec{r}-\vec{r}\,'|}\right) + \frac{1}{|\vec{r}-\vec{r}\,'|}\left(\vec{\nabla}_{\vec{r}\,'}\vec{j}(\vec{r}\,',t_{ret})\Big|_{t_{ret}} + \partial_{t_{ret}}\vec{j}(\vec{r}\,',t_{ret})\vec{\nabla}_{\vec{r}\,'}\,t_{ret}\right)\\ &= \vec{j}(\vec{r}\,',t_{ret})\frac{\vec{r}-\vec{r}\,'}{|\vec{r}-\vec{r}\,'|^3} + \frac{1}{|\vec{r}-\vec{r}\,'|}\left(\vec{\nabla}_{\vec{r}\,'}\vec{j}(\vec{r}\,',t_{ret})\Big|_{t_{ret}} + \frac{1}{c}\frac{\vec{r}-\vec{r}\,'}{|\vec{r}-\vec{r}\,'|}\partial_{t_{ret}}\vec{j}(\vec{r}\,',t_{ret})\right),\end{aligned}$$

which means that we can write

$$\vec{\nabla}_{\vec{r}}\,\frac{\vec{j}(\vec{r}\,',t_{ret})}{|\vec{r}-\vec{r}\,'|}+\vec{\nabla}_{\vec{r}\,'}\,\frac{\vec{j}(\vec{r}\,',t_{ret})}{|\vec{r}-\vec{r}\,'|}=\frac{\vec{\nabla}_{\vec{r}\,'}\vec{j}(\vec{r}\,',t_{ret})\Big|_{t_{ret}}}{|\vec{r}-\vec{r}\,'|}.$$

Plugging in this into (B.1) yields

$$\vec{\nabla}\vec{A}+\frac{1}{c^2}\frac{\partial\varphi}{\partial t}=\frac{\mu_0}{4\pi}\int_V -\vec{\nabla}_{\vec{r}\,'}\,\frac{\vec{j}(\vec{r}\,',t_{ret})}{|\vec{r}-\vec{r}\,'|}+\underbrace{\frac{\vec{\nabla}_{\vec{r}\,'}\vec{j}(\vec{r}\,',t_{ret})\Big|_{t_{ret}}}{|\vec{r}-\vec{r}\,'|}+\frac{\partial}{\partial t}\frac{\rho(\vec{r}\,',t_{ret})}{|\vec{r}-\vec{r}\,'|}}_{=0\text{ due to continuity equation}}\,\mathrm{d}\vec{r}\,'.$$

For the remaining first term we use *Stokes Law*

$$\vec{\nabla}\vec{A}+\frac{1}{c^2}\frac{\partial\varphi}{\partial t}=-\frac{\mu_0}{4\pi}\int_V\vec{\nabla}_{\vec{r}\,'}\,\frac{\vec{j}(\vec{r}\,',t_{ret})}{|\vec{r}-\vec{r}\,'|}\mathrm{d}\vec{r}\,'=-\frac{\mu_0}{4\pi}\oint_{\partial V}\frac{\vec{j}(\vec{r}\,',t_{ret})}{|\vec{r}-\vec{r}\,'|}\mathrm{d}\vec{\sigma}=0,$$

because the current density vanishes at infinity. That's what we wanted to show.

C

Softwarestack

D

Code Documentation

E

Normalization

List of Figures

Bibliography

[1] M. P. Allen and D. J. Tildesley. *Computer Simulation of Liquids*. Clarendon Press, New York, NY, USA, 1989.

[2] J. P. Boris. Relativistic plasma simulation-optimization of a hybrid code. *Proceeding of Fourth Conference on Numerical Simulations of Plasmas*, November 1970.

[3] A.Bruce Langdon Charles K. Birdsall. *Plasma physics via computer simulation*. IOP, 1991.

[4] C. Herzing. *Die molekulardynamische Simulation strahlender Plasmen*. 2016.

[5] Christian Kanzow. *Numerische Mathematik II*. 2005. [Online; accessed 13-Oktober-2016].

[6] W. Nolting. *Grundkurs Theoretische Physik 3:*. Grundkurs Theoretische Physik / Wolfgang Nolting. Springer, 2004.

[7] A. Taflove and S.C. Hagness. *Computational Electrodynamics: The Finite-difference Time-domain Method*. Artech House antennas and propagation library. Artech House, 2005.

[8] Kane S. Yee. Numerical solution of initial boundary value problems involving maxwell's equations in isotropic media. *IEEE Trans. Antennas and Propagation*, pages 302–307, 1966.

Declaration

Erklärung:

Hiermit erkläre ich, die vorliegende Arbeit selbständig verfasst zu haben und keine anderen als die in der Arbeit angegebenen Quellen und Hilfsmittel benutzt zu haben.

München, Datum der Abgabe

München, 18.07.2017, David Symhoven